
# Rapid distinction of dumpsite objects using Multiple-Aspect Scattering - Results from scaled tank experiments

P. Blondel

University of Bath, Department of Physics, Claverton Down, BA2 7AY Bath, UK
pyspb@bath.ac.uk

Toxic dumpsites on the seafloor are causing increasing environmental concern, but traditional sonar imaging strains to distinguish objects in unconsolidated sediments, in particular in cluttered terrains. Scaled tank experiments were conducted with 4 different cylinders (fluid-filled and solid aluminium, air-filled and solid stainless steel, respectively) and 2 seabed types (silt and gravel), using the facilities at the University of Bath. The setup was a 10:1 scaled version of the EC-SITAR sea trials site in the Stockholm Archipelago (Sweden). The main aim of these experiments was to design efficient surveying strategies, later used at sea. Our studies showed large variations depending on the aspect of these targets and their bistatic imaging configuration. These variations can be directly related to the shapes of the targets (e.g. dimensions, presence of ribs), their content (hollow or solid) and the material of the shells (e.g. stainless steel or aluminium). They are quantified using the combined $L^4$ norm of the time-domain signals at each aspect. Using appropriate ranges of multistatic configurations and imaging each target at 3 distinct aspects (45° apart), it is possible to successfully distinguish between similar targets with distinct contents and/or material, even in cluttered terrains.

# 1 Background

The seafloor has been one of the most convenient sites where to dump bulk chemical ammunition, toxic waste and radioactive products, from industrial or military sources, during most of the previous century. This is now prohibited by the London Convention (1975), not always respected. Because of pressing environmental concerns, such as contaminants leaking into the surrounding biota or immediate risk from exposure to the waste (e.g. when trawling), there have been growing efforts to locate these dumpsites and assess the risks they cause. The location problem is compounded by the fact that most of the waste has undergone partial or complete burial. Even when properly documented, it is not always located where it was laid, either because of dispersal during the dumping process or because of bottom currents and sediment redistribution.

Traditional tools such as sidescan sonar can produce accurate maps of objects proud on the seabed or partly buried if imaged in appropriate conditions [1,2]. More recent tools, such as Parametric Synthetic-Aperture Sonar [3] can identify and map potential dumpsites with targets buried down to 1 m. But there is still no sure way to distinguish targets from their backscatter characteristics alone. This is particularly problematic in large areas (e.g. the Farallon Island Radioactive Waste Dump, where 47,800 barrels are scattered over 1,400 km$^2$) [1] and in dense and cluttered environments (e.g. the Möja Söderfjord dump site, where 450 targets occur in a few hundred m$^2$) [4]. In most areas, the targets are too deep or sedimented, or the water is too opaque, to allow time-consuming optical recognition of each individual object.

Many theoretical studies (e.g. [5-8]) and a significant number of experiments (e.g. [9-12]) showed the information necessary to identify and distinguish targets was contained in the full 3-D scattered acoustic field. Natural objects (e.g. rocks and boulders) do not exhibit the strong coherent structural waves characteristic of man-made objects (e.g. mines or, in our case, waste). The European SITAR project [13] used this 3-D structure by imaging target(s) with variable source and receiver geometries. Scaled experiments were used to prepare for the sea trials and identify the optimal geometries. Their analysis is presented here in the context of rapid target recognition, using information from previous studies [14] and from the sea trials themselves [3].

# 2 Scaled Tank Experiments

The experiments were conducted in the Bath tank facilities. The setup was designed to be a scaled version of the SITAR sea trials site in the Stockholm Archipelago (Sweden), with a scaling factor of approximately 10:1 (Fig. 1). The underground tank was 5.00 m x 1.54 m, with a constant water depth of 1.475 m. Sediment trays at the bottom included silt and fine gravel, 14 cm deep and thoroughly degassed. The 238-kHz imaging transducer had at a fixed incidence angle of 45°, 0.5 m from the target. The scattered signal was measured with a B&K-8103 hydrophone, mounted on a robotic system giving access to 111 scattering angles from 21.8° to 73° (counted positively from the bottom up). The output signal was amplified, band-pass filtered and averaged over 100 waveforms. The waveforms were all measured over the same amount of time from the transmission of the incident pulse. They were normalised to the amplitude of the direct arrival, to account for differences in source level and/or different propagation paths. They were then zero-banded to remove the direct signal and their envelopes were calculated using the Hilbert transform. More details are available in [9].

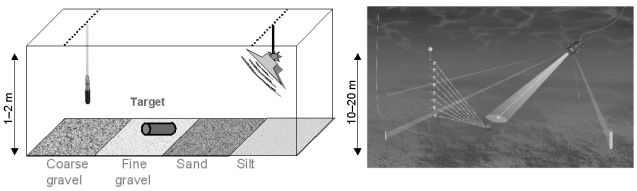


Fig.1 Scaled tank experiments (left) were used in preparation for full-scale sea trials (right).

The targets are scaled versions of typical marine waste containers (Fig. 2). They include aluminium cylinders of comparable dimension, one fluid-filled with small ribs (target $T_1$) and the other solid (target $T_3$), and stainless steel cylinders, one air-filled (target $T_2$) and the other solid (target $T_4$). Other targets were used for comparison with numerical simulations and with sea trials, but are not presented here as they do not show the complementary differences in material or in content of targets $T_1$-$T_4$. Each target was imaged at 3 horizontal aspects, noted respectively $T_x$ (along the X-axis of the imaging beam, i.e. end-on), $T_y$ (along the Y-axis of the imaging beam, i.e. broadside-on) and $T_{xy}$ (diagonal).

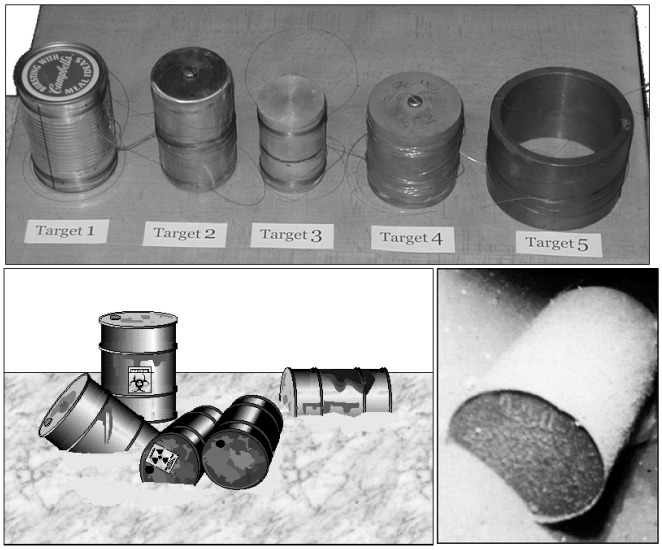


Fig.2 The targets used in these experiments (top) were scaled versions of those usually encountered in marine dumpsites, e.g. oil drums and radioactive waste (bottom).

# 3 Target Analyses

## 3.1 Bistatic scattering strengths

Targets are traditionally analysed by looking at their bistatic scattering strengths, using the standard sonar equation. Targets $T_1$ and $T_3$ in the present dataset were analysed by [15-16] for various aspects and, for vertical targets only, for different degrees of burial (proud, half-buried, flush-buried). Scattering strengths vary with aspect and burial, and it was possible to distinguish between hollow and solid aluminium cylinders on silt using measurements at three aspect angles 45° apart.

The sonar equation requires knowing the calibration of both projector and receiver(s), as well as the exact positions of the instruments and the target.. The size of the bistatic scattering area is modulated by the pulse length and the positions and directionalities of source and receiver. Not using the sonar equation can be useful when one of the instruments is not properly calibrated, or when some parameters are unknown (e.g. positions, beam patterns, seafloor tilt) [17]. An alternative analysis technique should therefore be able to compare signals acquired with the same sonar over separate targets, but during the same survey.

## 3.2 Frequency-domain analyses

Bistatic scattering strengths reduce the scattering from a target to a single number, associated to the main scattering. But subtler changes are visible in the entire waveforms, associated to possible internal reflections within the target, variations in contents and/or interactions with the seabed, and they can prove essential in distinguishing between targets. We previously investigated the frequency-domain variations between signals scattered by two targets of the SITAR dataset ($T_1$ and $T_2$, imaged end-on and broadside-on) [14]. Using the Log Spectral Deviation between two signals, we verified that the 3-D acoustic field scattering does indeed provide additional information that can be successfully exploited in target classification. We also showed that in some cases, strictly bistatic configurations (one angle of incidence, one angle of scattering) are not sufficient and multistatic configurations (one angle of incidence, several angles of scattering) should be preferred. This technique required the computation of the distance to the background sediment (without targets). This can easily be achieved in the laboratory by removing the target; at sea, it assumes the sediments around the targets do not change too rapidly and can be measured on their own. The role played by the seabed is not negligible, and although [14] distinguished between two dissimilar targets (fluid-filled aluminium vs. air-filled stainless steel) proud on silt, it was not possible to distinguish them on the gravel background.

## 3.3 Time-domain analyses

Both analyses of the bistatic scattering strengths [15] and of the frequency-domain distances between targets [14] show large variations depending on the aspect (*x*, *xy* or *y*) of these targets. These variations are directly related to the shapes of the targets (e.g. dimensions, presence of ribs), their content (hollow or solid) and the material of the shells (e.g. stainless steel or aluminium). They confirm the theoretical comparisons of [18], showing that the scattering from a solid cylinder in free space is marked by a large number of regular sidelobes a few degrees wide, and those of [19] on time-domain scattering by different targets.

Similar observations were made in studies limited to multi-aspect backscattering [12,19]. [12] argued in particular that natural objects (e.g. rocks and boulders) do not exhibit the strong coherent structural waves characteristic of man-made objects (e.g. mines or, in this case, waste containers). These elastic waves are strongly aspect- and object-dependent and could be used to distinguish between targets. Comparing signals from distinct targets should therefore use very different aspects, to maximise potential variations. This is the case in the present experiment, where the aspects measured cover broadside, end-on and diagonal emplacements. The exact orientation of a target on the seabed is not always known *a priori*, for example if too small to be properly resolved by the original sonar survey. For this reason, an equal weight must be given to the contributions from each aspect.

To investigate the differences between time-domain waveforms, we use earlier analyses of the bistatic scattering strengths of targets $T_1$ and $T_3$ by [16]. These targets could be distinguished from the combination of their contributions at three different orientations 45° apart, using the simple norm:

$$|T| = \sqrt{|T_x|^2 + |T_{xy}|^2 + |T_y|^2} \qquad (1)$$

where $|T_x|$, $|T_{xy}|$, $|T_y|$ are the bistatic scattering strengths calculated at each scattering angle. We propose to extend this norm to raw waveforms, by replacing the aspect-specific value $|T_\alpha|$ (for aspect $\alpha$, i.e. one of the three angles, separated by 45°, at which the target was imaged)) with the $L^p$ norm of the time-domain signal:

$$|T_\alpha| = \left( \sum_t |T_\alpha(t)|^p \right)^{\frac{1}{p}} \quad (2)$$
$$(p \geq 1); (\alpha = x, xy, y)$$

where $t$ is the time of measurement (thus summing over the entire waveform acquired), and $p$ is the power of the norm used. Each target will still be described by the parameter $|T|$ of Eq. (1), with one value for each combination of incidence angle and scattering angle (amounting to 111 values per target in this study).

The norm of each signal varies slightly with the power $p$ of the norm; differences become slightly significant only for $p$ = 2-4. The $L^4$ norm amplifies the differences between solid targets made of different materials (i.e. $T_1$ vs. $T_2$, $T_2$ vs. $T_4$) and is therefore selected. The difference between very distinct targets (different material, different content) will always be clear, whichever norm is chosen. All norms also clearly show the difference between solid and hollow targets made of identical material (i.e. $T_1$ vs. $T_3$, $T_2$ vs. $T_4$). The targets can always be separated clearly from the seabed (silt or fine gravel), the norms of the scattered signals being 1.2-4 times higher at all scattering angles.

## 3.4 Applications

The comparisons between the $L^4$ norms of different targets are presented in Fig. 3 (for targets proud on a silt seabed) and in Fig. 4 (for targets proud on a fine gravel seabed). Each time, the ratios investigated corresponded to: (top graph) targets made of the same material but with a different content (i.e. solid vs. fluid- or air-filled); (middle graph) targets either both solid or both hollow but made of different material (i.e. aluminium vs. stainless steel) and (bottom graph) completely distinct targets.

Targets placed proud on the silt seabed are easily distinguishable in most cases (Fig. 3). There is a clear difference between each side of the near-specular angle (~ 45°). When the scattering angle is smaller than ~42°, the differences between targets are smaller (~15%) and vary less with the scattering angle at which they are measured. Conversely, when the scattering angle is larger, the differences between targets are higher (up to 40%-60%) and show sharp peaks, 2°-4° wide. For targets made of the same material, but with a different content, one can observe that the values of $|T|$ are consistently larger for target $T_1$ than for $T_3$, with distinct peaks at 3-4° intervals between 44°-62°. The main differences between these targets are the content (fluid for $T_1$, solid for $T_3$), which accounts for higher scattering for $T_1$ [16] and the presence of small ribs at the surface of $T_1$ (although [16] showed their influence is more visible when scattering is measured away from in-plane). The higher visibility of the difference beyond the specular angle was also observed in analyses of the bistatic scattering strengths [16]. The difference between targets $T_2$ and $T_4$ is more contrasted. Below the near-specular angle, the solid target ($T_4$) scatters more (as much as 40% around 42°), and beyond the near-specular angle, the hollow target ($T_2$) scatters more (as much as 35% around 52°). This could be explained by different scattering mechanisms within the targets (i.e. internal reflections, visible on the raw waveforms) and different interactions with the neighboring seabed, influenced by the proximity (or not) to the specular angle. The difference between the two hollow targets is quasi-constant ($T_1$ scattering 15% more than $T_2$) at nearly all angles, except just before the near-specular angle, where the measurements of $T_1$ are up to 45% higher than those of $T_2$. Analyses of the raw waveforms correspond to stronger internal reflections. The difference between the two solid targets is more subdued but mirrors the pattern of the differences between $T_1$ and $T_2$. The measurements for $T_4$ are higher (ca. 25%) at broad peaks centered on 54° and 61° respectively, and smaller (ca. 25%) at 66° only. The physical reason for these differences must lie in the high density contrast (2.7 g/cm$^3$ for $T_3$, 7.8 g/cm$^3$ for $T_4$) or as the slightly shorter diameter of $T_3$ was not seen to increase the broadside contribution to $|T_3|$. Finally, the differences between two dissimilar targets will be significant at scattering angles higher than 30° and definitely higher (30-40%) beyond the near-specular angle.

Targets placed on the gravel seabed should be harder to detect, because of the higher surface roughness of the background and the contribution of many facets to the full 3-D scattering. Indeed, overall, the measurements of $|T|$ are smaller on the gravel background (20-30% smaller than for silt). But the targets are still easily distinguishable, and the variations with scattering angle mirror those observed for the silt background (Fig. 3). Differences between targets will be higher for scattering angles beyond the near-specular angle. The measure of $T_1$ shows a sharp loss (74%) at a scattering angle of 35°, and $T_4$ experiences a smaller loss (40%) at 41°, the only effects of which are to make them less distinguishable at these specific angles. Closer analyses of the individual waveforms show these losses are associated to interactions with the gravel. An interesting change from the silt background is that, at lower scattering angles (ca. 30°-35°), the differences between targets made of the same material and between hollow/solid targets are amplified by up to 30%. For all targets, the contributions to $|T|$ systematically come mostly from the $x$ and $xy$ aspects, i.e. from interactions within the targets (presenting their long axes to the imaging beam).

Investigations of other bistatic angles revealed that the differences between targets were amplified when the bistatic angle was 10° either side from in-plane, and decreasing again at 20°, presumably because of the angular width of the imaging beam relative to the target, and the influence of small-scale variations at target surfaces [16]. But these differences were not systematic, and the lack of comparable data for targets on gravel meant that bistatic angle variations were not investigated further.

The general conclusions are that there is no specific scattering angle, i.e. no unique bistatic configuration, which offers unambiguous distinction between targets, but rather definite ranges of scattering angles over which the targets can be distinguished. These ranges will depend on the background. For a silt background, the targets are more easy to distinguish from each other, whether they are made from the same material but have different content, or of similar content but made from different material, for scattering angles beyond the near-specular angle (45° in this case). The same targets, placed on a gravel background, will be less easy to distinguish, but their differences will be amplified at scattering angles close to 30°, presumably because of interactions with the rough and more reflective seabed.

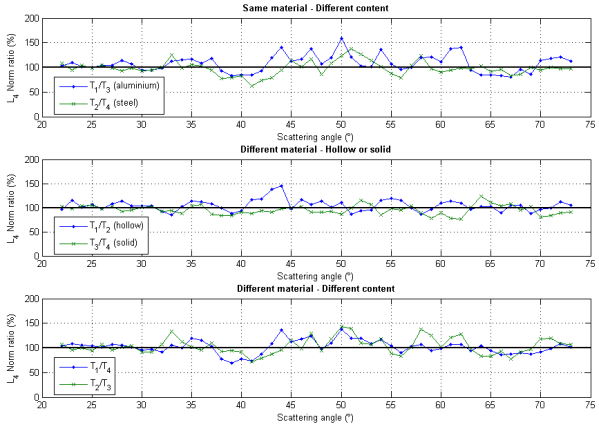


Fig.3 Variations of the $L^4$ norms of signals scattered by targets placed proud on silt. The thick black line shows the 100% level, i.e. when the targets have the same response.

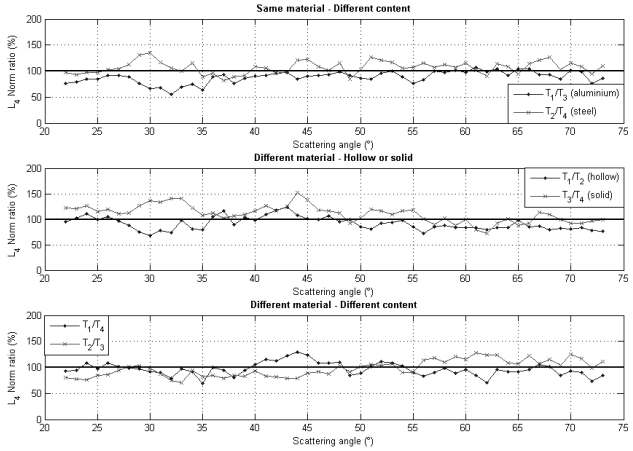


Fig.4 Similar diagrams for targets placed proud on gravel.

combined DGPS and an acoustic baseline. These measurements allowed acquisition of multistatic scattering measurements over a range of scattering angles centred on the specular direction. In the real world, the targets of interest will be varied but based around the same characteristics. Contrary to mines, which are shaped to be covert and made of materials minimising their acoustic signatures, dumpsite objects should be easier to find. The examples of Fig. 2 show for example prominent ribs (e.g. on oil drums) and lids that can come up loose, possibly spilling contents on the seabed. These contents can be radioactive sludge or objects (encased in bitumen/concrete for low-level waste) or closely-packed shells (for ammunition). Dumpsite objects will also usually appear in groups, at least at the scale of the sonar used in general dumpsite mapping. The position of the receivers can then be set at the optimal distance to get good angular and temporal separation for the returns from each target. It is possible to isolate the portion of the signal corresponding to each target, and use the technique presented in Section 3. This is possible for targets placed 1 diameter and/or 1 length apart from each other, in clusters of up to 5 targets [9].

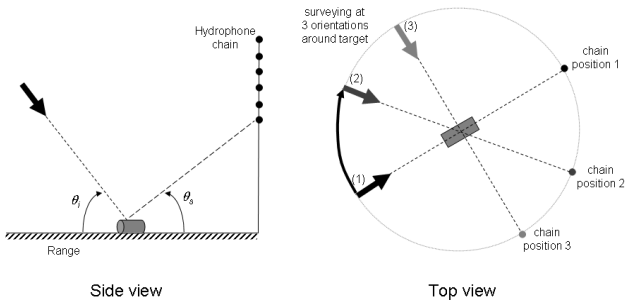


Fig.5 Proposed geometries for Multiple-Aspect Scattering surveying and distinction of targets with their $L^4$ norm.

# 4 Extension to Sea Trials and Marine Dumpsites

The results of the previous section have direct implications in the planning of a marine dumpsite survey strategy. Although they are limited to 4 different targets, and 2 types of seabed, the results from Section 3 showed the distinct nature of these targets can be clearly identified by measuring the multistatic scattering of each target at 3 aspects (Fig. 5) and combining these measurements with a simple metrics (Eq. 2). This can be performed by placing the imaging sonar on a ROV, and measuring at several suitably placed scattering angles (with a series of hydrophones on a vertical chain, in line with sonar and target, or with another vehicle moving the hydrophone(s) to the desired locations). This surveying approach was part of the multiple-aspect geometries adopted during the SITAR sea trials at the Möja Soderfjärd dumpsite [4]. In this case, a parametric sonar TOPAS-120 was placed on the *Plums* ROVand rotated around the objects of interest. The imaging beam was very narrow (3-4°). Scattering was measured on a hydrophone chain, made of 8 omnidirectional elements 2-m apart. Varying hydrophone separations, scattering angles between 20° and 40° could be achieved. Exact positioning

# 5 Discussion Conclusion

The experiments presented here were a scaled version of a surveying set-up later used at sea. They used 4 targets of comparable dimensions (fluid-filled and solid aluminium cylinders, air-filled and solid stainless steel cylinder), placed proud on 2 types of seabed (silt and fine gravel). These targets were imaged at 238 kHz, at 3 different aspects (broadside on, end-on and diagonal). The incidence angle was fixed at 45° and 111 scattering angles measured between 21.8°-73°. Bistatic angles of 10° and 20° were also investigated for targets on the silt background. To quantify the difference between targets, a simple metrics combining the $L^4$ norm of the time-domain measurements over the 3 aspects was designed. All targets can be distinguished from each other using this norm, whichever background they are placed on. Targets made of a similar material but with differing contents can be distinguished. Targets with similar content but made of different materials can also be distinguished. There is no specific scattering angle at which all targets can be distinguished, but a range of angles beyond the specular direction (for both silt and gravel). This range encompasses low scattering angles in the case of gravel, rough and reflective. These results confirm and extend the observations of [14], quantifying the scattering

of 2 targets in 2 aspects using a different approach but not resolving them in gravel. It is possible to distinguish targets, imaged at 3 aspects oriented 45° from each other. This can greatly simplify the surveying of dumpsite objects, alone or in clusters. A problem often identified in short surveys is the complexity and time taken for simple identification procedures [3]. Although it cannot at the moment unambiguously identify the make-up of individual targets, the technique presented here can at least distinguish between target types. Understanding which aspects of the targets contribute to the $L^4$ measurements for which range of angles will be able to draw from the large body of experience on the multi-aspect backscatter of mine-like objects [12,20-22]. Although the targets are different, and the scattering geometries are different, theoretical work [8] and detailed analyses [23] showed the main contributions were specular reflection, geometric diffraction effects and structural response (particularly for symmetrical man-made targets). The approach presented here uses the time-domain signals with minimum processing. No assumption is made about the targets (e.g. symmetric shapes) or the scattering processes (e.g. Lamb waves). The shapes of dumpsite objects can vary considerably depending on the mode of disposal and later evolution (e.g. impacted sides, open lids, corroded sections). The contents of dumpsite objects will also vary, in type (e.g. radioactive waste or chemical shells) and in amounts (e.g. leaking or empty drums). The backscatter of partially fluid-filled stainless steel cylindrical shells was measured by [24], showing steady changes in form functions and adding resonance features for the larger amounts of water. Future research should isolate plausible end-members for shape and content variations of dumpsite objects, and assess how their $L^4$ measurements can optimise the bistatic surveying strategies. Current investigations use a wider range of bistatic configurations, from tank experiments and sea trials.

# References


[1] H.A. Karl, W.C. Schwab, D.E. Drake, J.L. Chin, USGS Open-File Report 92-178 (1992)

[2] Ph. Blondel "Automatic mine detection by textural analysis of COTS sidescan sonar imagery", *Int. J. Rem. Sens.*, 21(16), 3115-3128 (2000)

[3] M. Zakharia et al. "Acoustical methods", *Buried Waste in the Seabed*, 179-182, (2007)

[4] P. Moren et al. "Acoustic sea trial in the Möja Söderfjärd dumpsite", *Buried Waste in the Seabed:* 87-101 (2007)

[5] H. Schmidt et al., "GOATS'98: bistatic measurements of target scattering using autonomous underwater vehicles", SACLANTCEN Rep. SR-302, 1998

[6] I. Karasalo, J. Hovem, "Transient bistatic scattering from buried objects", in *Experimental Acoustics Inversion Methods*, 161-176, 2000

[7] F.J. Blonigen, P.L. Marston, "Leaky helical flexural wave backscattering contributions from tilted cylindrical shells", JASA 112(2), 528-536 (2002)

[8] M. Zampolli, et al., "Finite element and hybrid modelling tools for the detection and classification of buried objects in shallow-water", *Boundary influences high-frequency shallow-water acoustics*, (2005)

[9] Ph. Blondel, et al.; "Scaled multiple-aspect scattering tank experiments", *Buried Waste in the Seabed* (2007)

[10] K.L. Williams et al., "Underwater sand acoustics: A perspective derived from the sediment acoustics experiment (SAX99)", J. Acoust. Soc. Am., 113(4), 2298 (2003)

[11] M.D. Richardson et al., "The effects of seafloor roughness on acoustic scattering", *Boundary Influences in High-Frequency Shallow Water Acoustics,* (2005)

[12] M. Montanari et al., "AUV-based concurrent detection and classification of buried targets using higher order spectral analysis", IEEE JOE, 31(1), 188-199, 2006

[13] A. Caiti et al., *Buried Waste in the Seabed*, 73-78 (2007)

[14] M. Cosci, et al, "A potential algorithm for target classification in sonar bistatic geometries",

[15] Ph. Blondel et al., "High-frequency bistatic imaging of proud targets – Influence of target orientation and type", Proc. 2nd UAM, Heraklion (2007)

[16] Ph. Blondel, "High-frequency bistatic scattering from small targets", IEEE JOE, submitted (2007)

[17] R.P. Howey, Ph. Blondel, this volume, 2008

[18] A.T. Abawi, M.B. Porter; "The use of the equivalent source technique in the calculation of scattering from underwater targets", *Boundary influences in high-frequency shallow-water acoustics*, 341-347, (2005)

[19] S. Ji, X. Liao, and L. Carin, "Adaptive multi-aspect target classification and detection with hidden markov models," in *Proc. Int. Conf. Acoustics, Speech and Signal Processing*, vol. 2, May 2004, pp. 125–128.

[20] Schmidt, H., J. Lee; "Physics of 3-D scattering from rippled seabeds and buried targets in shallow water", J. Acoust. Soc. Am. 105, 1605-1617 (1999)

[21] Dong. Y., P. Runkle, L. Carin; "Markov modelling of transient scattering and multi-aspect target classification", Proc. ICASSP'01, 2841-2844, (2001)

[22] Robinson, M., M.R. Azimi-Sadjadi, D.D. Sternlicht, D. Lemonds; "Multi-aspect acoustic classification of buried objects", Proc. OCEANS'2003, 474-484, 2003

[23] A. Tesei et al, "Measurements and modeling of Acoustic Scattering from Partially and Completely Buried Spherical Shells", JASA 112 (5), 1817-1830, (2002)

[24] Humphrey, V.F., N. Jayasundere, M. Dench, P.A. Chinnery, "Experimental and theoretical studies of scattering by partially fluid-filled cylindrical shells", Proc. ECUA-2004, 463-468 (2004)